Journal of Catalysis 268 (2009) 290–296

Contents lists available at ScienceDirect

Journal of Catalysis

journal homepage: www.elsevier.com/locate/jcat

SAPO-34 methanol-to-olefin catalysts under working conditions: A combined *in situ* powder X-ray diffraction, mass spectrometry and Raman study

David S. Wragg [a,d,*], Rune E. Johnsen [a,d], Murugan Balasundaram [a,d], Poul Norby [a,d,1], Helmer Fjellvåg [a,d], Arne Grønvold [b,d], Terje Fuglerud [b,d], Jasmina Hafizovic [c,d], Ørnulv B. Vistad [c,d], Duncan Akporiaye [c,d]

[a] *Centre for Materials Science and Nanotechnology and Department of Chemistry, University of Oslo, Sem Sælands vei, N-0315 Oslo, Norway*
[b] *Ineos Chlorvinyls Hydrovegen 53, 3936 Porsgrunn, Norway*
[c] *SINTEF Materials and Chemistry Forskningsvn 1, N-0314 Oslo, Norway*
[d] *InGAP Centre for Research Based Innovation*

ARTICLE INFO

Article history:
Received 15 July 2009
Revised 25 September 2009
Accepted 29 September 2009
Available online 23 October 2009

Keywords:
Catalysis
Methanol-to-olefin
Zeolite
SAPO-34
In situ X-ray diffraction
Mass spectrometry
Raman

ABSTRACT

We have studied the behaviour of the zeotype silicoaluminophosphate SAPO-34 catalyst in the methanol-to-olefin (MTO) process under real working conditions using simultaneous synchrotron powder X-ray diffraction (PXRD) and Raman spectroscopy with online analysis of products by mass spectrometry. Anisotropic changes in the unit-cell dimensions are shown to be related to the build-up of intermediate species in the cages of the SAPO-34 framework and also to the deactivation of the catalyst (observed from the products in the mass spectra). We have quantified the amount of intermediate material in the cages from the PXRD using Fourier mapping techniques and our measurements are comparable with tapered element-oscillating microbalance measurements of coke build-up. Raman spectra indicate that the nature of the coke becomes increasingly graphitic with time. Our results also show that the catalyst recovers its original structural parameters when regenerated in air at 500–550 °C.

1. Introduction

The methanol-to-olefin (MTO) process allows the production of some of the most valuable chemical building blocks from biomass, natural gas or coal [1]. The process is catalyzed by acidic zeotype frameworks such as ZSM-5 and the silicoaluminophosphate SAPO-34. The latter offers a combination of favourable properties (especially high selectivity for light olefins) leading to commercial exploitation by UOP and INEOS (formerly Norsk Hydro) [2]. There right has been much research into the mechanism of the MTO conversion and the carbon pool mechanism first proposed by Dahl and Kolboe [3–5] is now widely accepted while recent work from Hereijgers et al. has shown that product rather than intermediate shape selectivity controls the reaction [6]. The deactivation of the catalyst is also of great interest (SAPO-34 requires regeneration after a few hours on stream) with increasing time on stream seeing higher levels of large aromatic compounds [7–9]. Recent work suggests that many of these may be formed after the deactivation of the catalyst when product diffusion out of the crystals is limited by coke [6,10].

Methods for the *in situ* study of chemical reactions using X-ray diffraction and scattering techniques that have been developed over the past few years have allowed observation of several types of reaction [11–15]. Synchrotron radiation is commonly used for this purpose as the high X-ray intensity available allows extremely rapid collection of good quality diffraction data, and it is becoming increasingly common to apply other techniques at the same time as collecting X-ray data with Raman spectroscopy being especially useful [16–18]. In this study we have utilized the combined time-resolved powder X-ray diffraction (PXRD), Raman and mass spectrometry setup available at station BM01A of the Swiss-Norwegian beamline (SNBL) of the European Synchrotron Radiation Facility (ESRF) [19]. We have observed significant changes in the unit-cell dimensions of SAPO-34 during the coking phase of the MTO process which appear to be linked to the build-up of intermediates in the large cages of the framework. This is supported by *in situ* analysis of the coke by Raman, which reveals increasing levels of graphitic material. Further analysis of the peak line width in the powder XRD data indicates that strain develops in the framework during the build up of intermediates but is released when they are removed by oxidative regeneration of the catalyst. An

* Corresponding author. Address: Centre for Materials Science and Nanotechnology and Department of Chemistry, University of Oslo, Sem Sælands vei, N-0315 Oslo, Norway. Fax: +47 22 85 54 41.
E-mail address: david.wragg@smn.uio.no (D.S. Wragg).
[1] Present address: Risø National Laboratory for Sustainable Energy, Technical University of Denmark, P.O. Box 49, DK-4000 Roskilde, Denmark.

0021-9517/$ - see front matter © 2009 Elsevier Inc. All rights reserved.
doi:10.1016/j.jcat.2009.09.027

experiment using discrete pulses of methanol rather than a continuous feed shows that active intermediates are used up quickly after each pulse leaving coke-like intermediates which grow in size over the sequence of pulses. These must be replenished with methanol in order to continue the production of alkenes.

2. Experimental methods

2.1. Combined in situ PXRD and Raman studies on the MTO process

The reactions were carried out in a flow cell based on a standard 0.7 mm quartz glass capillary containing approximately 2 mm^3 of SAPO-34 (8% silicon content, calcined in air at 550 °C for 24 h) synthesized by the method of Dahl et al. [20] packed between two plugs of quartz wool. A flow of 20 ml/min of helium saturated in methanol at 25 °C through a bubbler was used as the reactant feed, with a pure helium flow at the same rate used during preheating of the catalyst to the chosen reaction temperature. 20 ml/min of 10% oxygen in helium was used during the regeneration stages. The flow out of the reactor was measured at 3.5–5 ml/min. Synchrotron PXRD data were collected at wavelengths of 0.69402 and 0.69981 Å on a MAR 345 image plate detector with a time resolution of ~107 s and converted into conventional 1D powder patterns with FIT2D [21]. Raman data were collected simultaneously on a Renishaw system using a 532 nm green laser source (one spectrum from 100 to 3200 cm^{-1} was acquired every 55 s) and the product stream was analyzed with a Pfeiffer GSD-301-O1 Omnistar mass spectrometer scanning an M/e range of 4–70 with an acquisition time of 37 s.

PXRD patterns were analyzed using the Rietveld method with the program GSAS [22] and the EXPGUI interface [23]. Unit cells were refined in batch mode by a model-biased fit using the ALPO-34 framework [24] as a starting model. Fourier analysis was carried out on Rietveld refinements against the same starting model. The models were exported to the PLATON suite [25] in SHELX [26] format for calculation of the void electron count using the SQUEEZE algorithm. PXRD peak width, area and position analysis was carried out using the program Fityk [27] with O'Brien's script creating software [28]. Fityk was also used for fitting of the Raman peaks.

2.2. Tapered element oscillating microbalance (TEOM) measurements

Coking levels were monitored *in situ* in separate experiments using a TEOM. A SAPO-34 sample was placed in the reactor between quartz wool plugs and heated to reaction temperature in flowing He. Methanol was fed as saturated He, and nitrogen was added to the mixture to give a methanol partial pressure of 0.06 bar. The temperature was 450 °C and weight hourly space velocity (WHSV) was 70 g h^{-1}. An Agilent 3000 micro-GC was connected to the effluent for analysis of the effluent gas.

3. Results and discussion

3.1. PXRD of SAPO-34 during the MTO process

When the MTO process is run at 440 °C changes in both the intensity and position of the PXRD peaks are observed (Fig. 1).

Model-biased refinement of the unit cell and peak shape parameters of the rhombohedral SAPO-34 unit cell reveal that the change in the *a*-axis is small (*ca.* 0.1% contraction) while a significant change is observed in the *c*-axis (*ca.* 2%). When the reaction is carried out at 500 °C slightly larger changes are observed in both axes (3% change in *c*). When plotted against reaction time we speculate that the *c*-axis length reflects the progress of the reaction (Fig. 2) and the build-up of coke. The percentage changes in the axes are significantly greater than those found in the numerous studies of aromatic adsorption in ZSM-5 at room temperature [29–34]. The largest of these is a 0.5% increase in the *c*-axis when *p*-xylene is adsorbed [31] (we note that the structures reported by Mentzen and Gelin for the same loading of this adsorbate show a much lower level of expansion [30,33]). This suggests firstly that the framework of SAPO-34 is more flexible than that of ZSM-5 and secondly that the reaction causes greater strain in the cages than adsorbed aromatics. Further evidence of this is presented in Sections 3.3 and 3.4 below.

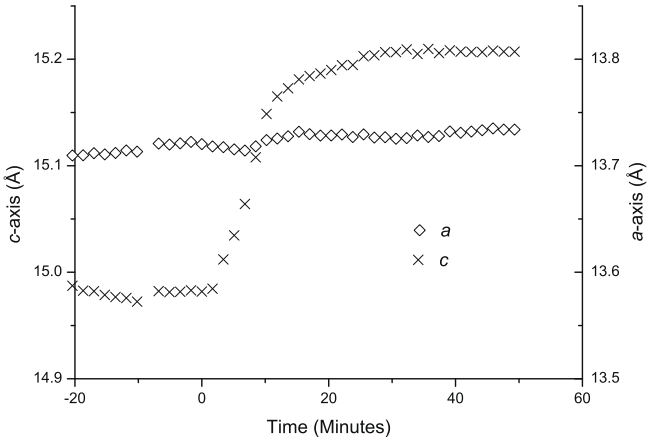

Fig. 2. Variation of the *a*- and *c*-axes of SAPO-34 during the MTO process at 450 °C. Time = zero corresponds to the first addition of methanol in this and all following graphs charting reaction progress against time. The estimated standard deviation error bars for the dimensions are smaller than the symbols used in the plots.

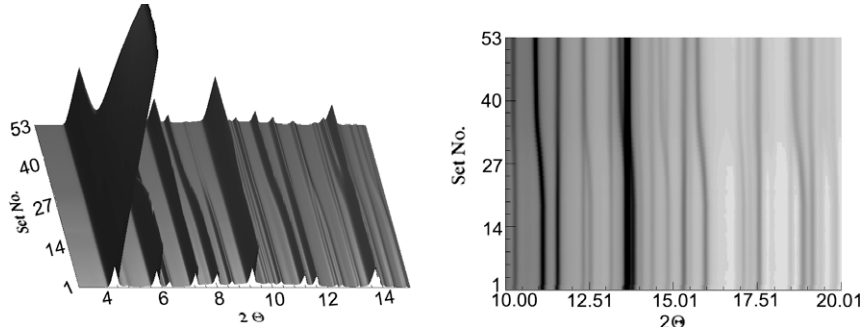

Fig. 1. (left) Three-dimensional stack plot of SAPO-34 PXRD patterns (2θ range 3–15°) collected during the MTO process at 440 °C, intensity changes are clearest in the initial (1 0 1) peak (2θ = 4.5°). (right) Film plot of the same data (2θ range 10–20°) showing peak position shifts which indicate anisotropic changes in the unit-cell dimensions. Time increases with set number.

3.2. Raman: the nature of the coke

The build-up of coke can also be observed in the Raman spectra collected during the process. Unfortunately due to the use of a 532 nm green laser source the majority of the spectral features are obscured by fluorescence. However, as the reaction progresses two broad bands at around 1415 and 1612 cm^{-1} can be discerned (Fig. 3left). In the *in situ* UV-Raman study of Li et al., the 1415 cm^{-1} is assigned to symmetric deformation of CH_x ($x = 2, 3$) species in the olefin products, with a band at 1632 cm^{-1} attributed to C–C bond stretching in olefinic coke [35]. Bands at 1604 cm^{-1} in the Raman spectrum of zeolite-Y under MTO conditions are assigned to aromatic species and we suggest that the 1612 cm^{-1} band in our spectra is due to the aromatic species, as observed in several other spectroscopic studies of MTO and methanol to hydrocarbon reactions [10,35–43]. The 1612 cm^{-1} band quickly broadens to a point where it can be fitted with two Gaussian peaks – one corresponding to the aromatics at around 1612 cm^{-1} and a second at 1570 cm^{-1} which is close to the value reported for the Raman signal of graphite (1583 cm^{-1}) [44] and some large polycyclic aromatics (assignments in Fig. 3right) [36].

Li et al. resolve the main aromatic C–C stretching peak in their spectra into bands at 1632 and 1620 cm^{-1}, and report that the peak is very broad and changes little with the reaction time; the broadening being due to polyaromatic species. Plotting the ratio of the graphitic to aromatic peak heights or areas in our data during the reaction shows a slight increase during the reaction (Fig. 4). This may be due to the build-up of graphitic surface species or very large polyaromatics. The former is supported by the recent work of Mores et al. [10] who used a combination of optical microscopy, UV/visible and fluorescence microspectroscopy on single crystals of ZSM-5 and SAPO-34 to track the formation of graphitic and aromatic coke species separately, showing that the formation of aromatic coke at the corners and edges of the SAPO-34 crystals was followed by the formation of larger coke compounds and graphitic deposits which block the diffusion path towards the centre of the crystal. This also fits well with our observation of an increasing ratio of graphitic to aromatic coke as the reaction progresses.

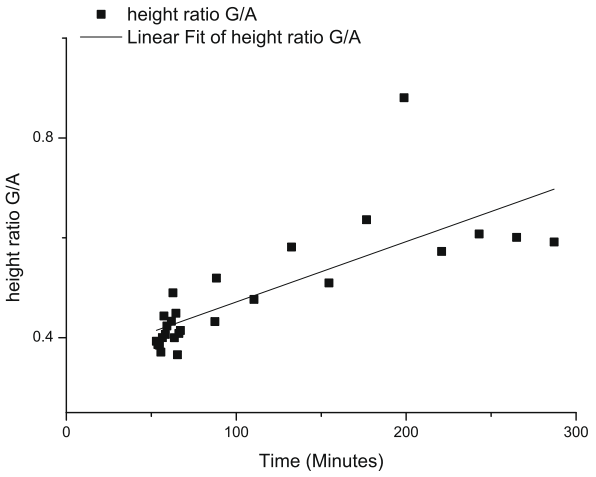

Fig. 4. Ratio of the peaks at 1585 cm^{-1} (G – graphitic) and 1612 cm^{-1} (A – aromatic) plotted against reaction time for the MTO process at 440 °C. The linear regression line shows the general upward trend in the graphitic:aromatic coke ratio.

3.3. Tracking the intermediates with difference Fourier mapping and TEOM

We have also tracked the build-up of intermediates in the cages with difference Fourier maps calculated from Rietveld refinements of the SAPO-34 framework against the powder patterns collected during the period of *c*-axis change. Difference Fourier maps allow us to compare the difference between the observed electron density and that described by the structural model. In this case the structural model used is the SAPO-34 framework, meaning that, to a first approximation, the electron density not described by this belongs to intermediates. Fig. 5 shows the residual electron density in the cages before switching on the methanol stream and then after 4 and 20 min. By 20 min a large cloud of residual electron density is visible in the cage.

Counting the residual electrons in the cages using the SQUEEZE algorithm and plotting these values against the reaction time gives a plot strikingly similar to that observed for the variation of the *c*-axis (Fig. 6).

We can make an approximate calculation relating the electron counts to the coke:framework mass ratio commonly used to describe the progress of the reaction in terms of coke build-up. If we assume that the coke is composed of hydrocarbons then we can (to a first approximation) take the molecular mass of coke in the unit cell to be double the number of electrons counted. The electron counts were adjusted to take into account a base level of the electron density counted before methanol addition and doubled to give approximate molecular masses of coke. These were then divided by the mass of the framework in the unit cell

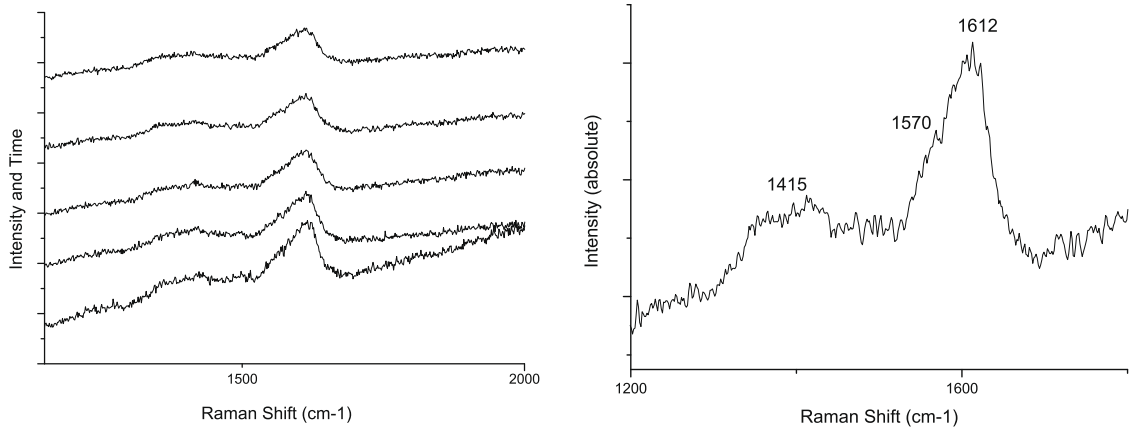

Fig. 3. (left) A series of Raman spectra for SAPO-34 during the MTO process (spectra summed over 5 min intervals from 5 to 25 min). In all cases the main peak at 1612 cm^{-1} shows broadening. (right) Positions of fitted peaks in the spectrum collected between 6 and 7 min after the addition of methanol at 440 °C (see Supplementary material for more details on fitting).

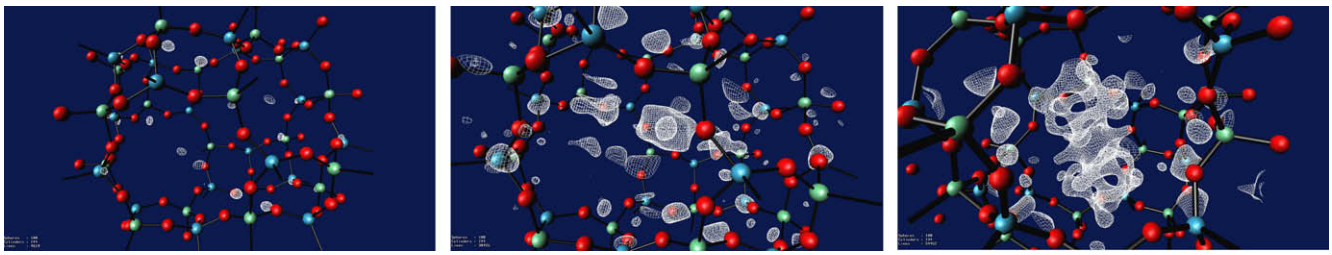

Fig. 5. Images of the residual electron density in the SAPO-34 cage, determined from difference Fourier maps. From left to right: 440 °C before reaction, 4 and 20 min into reaction. Red spheres = oxygen, green = phosphorus and blue = aluminium. The white contours represent residual electron density. (For interpretation of the references in colour in this figure legend, the reader is referred to the web version of this article.)

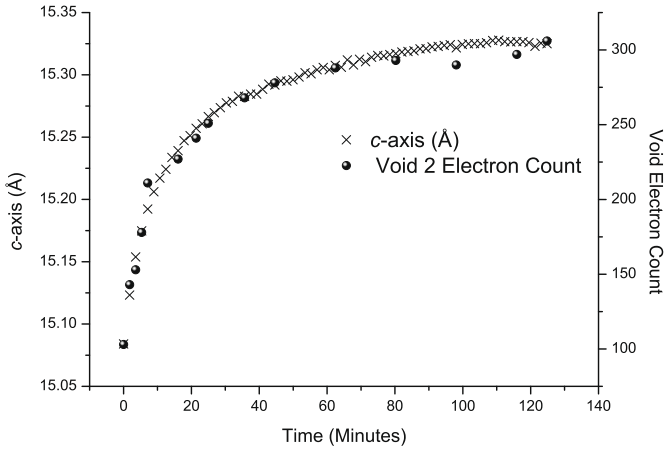

Fig. 6. Combined plot of the *c*-axis variation and void electron count of SAPO-34 during the MTO process at 440 °C. Methanol added at time = 0.

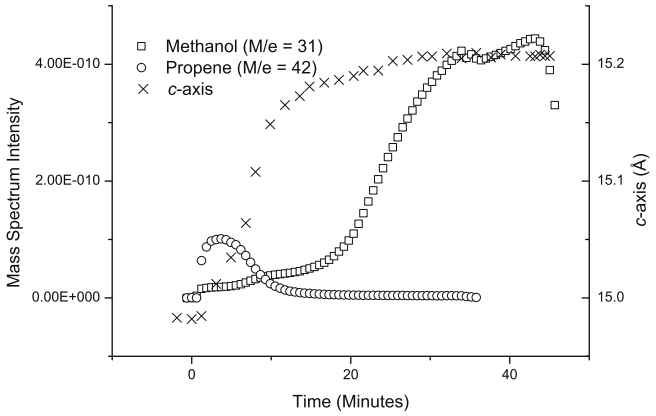

Fig. 8. Propene and methanol traces in the mass spectrum vs. time plotted alongside *c*-axis variation for SAPO-34 during the MTO process at 450 °C.

(2194.38 g mol^{-1}) to give ratios which agree well with those obtained in TEOM experiments at 450 °C (Fig. 7). The results also agree reasonably with those obtained by Bleken et al. using thermogravimetric analysis (TGA) [45].

The effect of coking on the product distribution can be observed in the mass spectra. Following the production of propene (*M*/*e* = 42), in the series of mass spectra a rapid increase in production rate is seen immediately after switching on the methanol stream. Decline in the rate of production begins six min after the methanol flow is switched on and follows a curve which is almost a mirror image of the *c*-axis increase (Fig. 8). This is in agreement with the previous results showing that coking reduces olefin production and leads to eventual deactivation of the catalyst [46]. Unreacted methanol (*M*/*e* = 31) does not start to come through the reactor until quite a late stage.

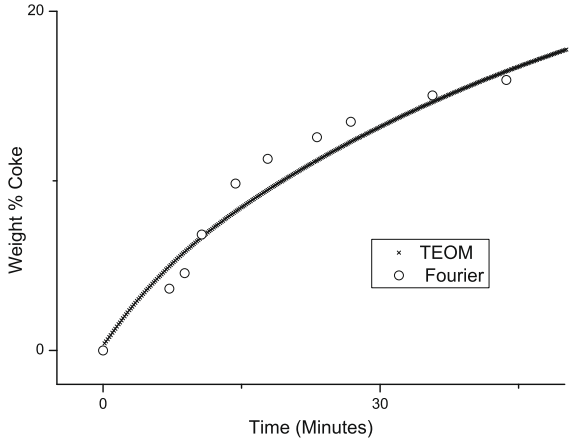

Fig. 7. Weight percentage of coke to catalyst calculated from the SQUEEZE electron counts and the mass of the framework unit cell plotted alongside the same ratio from TEOM measurements.

3.4. Using XRD line width to monitor strain in the catalyst structure

Line width analyses of the reflections were performed in order to investigate the influence of the coke on microstructural parameters. Assuming that there is no change in crystallite size the line width of a PXRD pattern gives an indication of the strain in the crystal lattice. Plotting the full width at half maximum (FWHM) for the (1 0 1) peak of SAPO-34 against time during the MTO process shows an increase which correlates to the *c*-axis expansion (Fig. 9). There is clearly a link between coke build-up, *c*-axis expansion and strain in the structure of SAPO-34.

FWHM increases steeply after the methanol addition reaching a peak and then declining slightly. The decline is thought to be due to a "chemical gradient" caused by inhomogeneous occupation of the SAPO-34 cages through the crystal lattice [47,48]. Once the cage occupancy is relatively consistent through the sample a settled value of FWHM is reached.

3.5. Varying reaction conditions and the effect of catalyst regeneration

The reaction was also studied at an increased pressure of 4 bar (the pressure was increased using a back pressure valve after the flow cell) at 440 °C. Interestingly the rate of *c*-axis increase at increased pressure seems to be lower compared to atmospheric pressure and the curve is very similar in shape to that obtained at atmospheric pressure and 430 °C (Fig. 10). This may suggest that

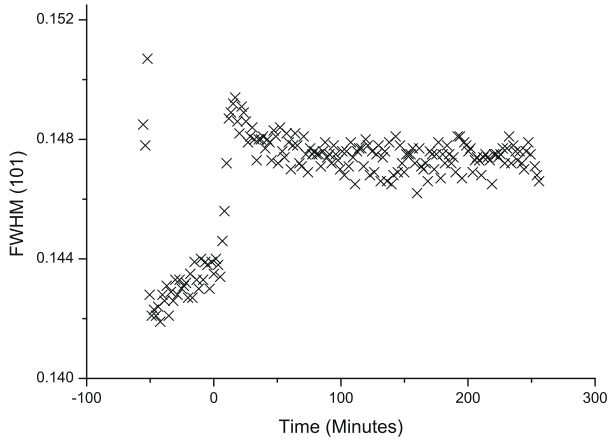

Fig. 9. FWHM of the (1 0 1) peak of SAPO-34 plotted against time during the MTO process at 430 °C. Methanol is added at time = 0. Changes before this time are due to dehydration and negative thermal expansion of the sample.

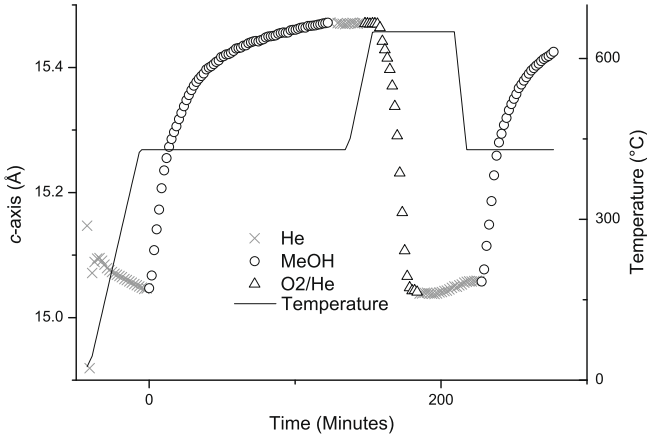

Fig. 11. Plot of *c*-axis against time for experiment 1 in the list above, in which the SAPO-34 catalyst was regenerated in 10% O_2/He. The different atmospheres used are denoted by the symbols used in the plots and the temperature is plotted alongside the data.

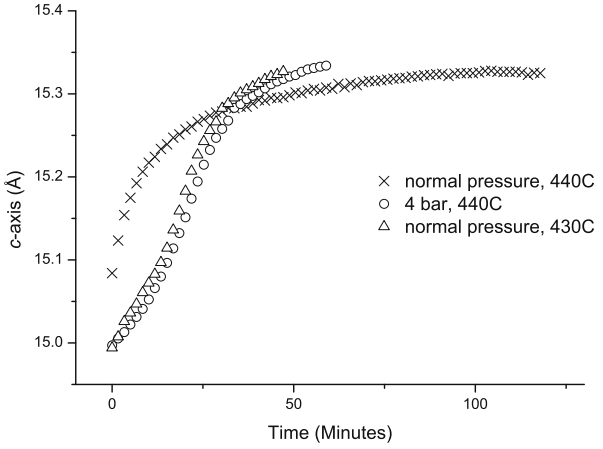

Fig. 10. *c*-Axis plots for SAPO-34 during the MTO process comparing the reactions at 430, 440 and 440 °C, 4 bar. Different shapes are probably caused by different flow rates through the cell.

these reactions have slightly different coking processes to the reaction at 440 °C and ambient pressure; however, it is most likely that the differences are due to variations in the flow rate through the reactor. We will see further evidence of this below.

Three experiments were carried out in which the SAPO-34 catalyst was regenerated and used for a second cycle of MTO conversion:

1. Conversion at 430 °C, regeneration at 650 °C, conversion at 430 °C.
2. Conversion at 360 °C, regeneration at 490 °C, conversion at 360 °C.
3. Conversion at 360 °C with ramp to 510 °C during the process, regeneration at 510 °C, conversion at 360 °C.

A plot of the *c*-axis during experiment 1 is shown in Fig. 11. In experiments 1 and 2, the *c*-axis returns to the original value of the calcined material while in experiment 3 the *c*-axis after regeneration is 0.03 Å longer than that at the start of the experiment. This may be attributed to incomplete regeneration – however it could also be a sign of some irreversible damage to the SAPO-34 framework caused by running the MTO process at 510 °C.

Sloping sections in the *c*-axis curves (see Fig. 12) near the end of the first coking in experiments 2 (75–125 min) and 3 (60–100 min) are probably caused by changes in the flow rate through the reactor due to coke build-up, which will in turn effect the rate of the reaction. Switching from methanol to helium flow at reaction temperature leads to a slight decline in the *c*-axis value. This is relevant to the pulsed experiment discussed below.

Plots of FWHM against time for the three experiments are shown in Fig. 12 and indicate that the strain built up in the structure is fully released on regeneration and in the case of experiment 1 the FWHM is even narrower after the first cycle of MTO conversion and regeneration (the opposite is true of experiment 3 because of incomplete regeneration or catalyst damage as discussed above).

Maxima in FWHM are again evident part way through the coking stage and also at the beginning of regeneration, supporting the theory that these increases in peak width are due to "gradients" in cage occupancy. In experiment 3 the change in temperature during the first cycle of MTO leads to a slight increase in FWHM but no peak suggesting that when this change took place all the active cages were occupied with intermediate species.

3.6. Experiments with a pulsed flow of methanol

A third type of experiment was performed in which 7 pulses of methanol were added to the reaction cell at 360 °C and allowed to react through. The first two pulses were 10 ml of methanol saturated helium, the following five 20 ml. The variation of the *c*-axis during the pulsed experiment is shown in Fig. 13.

Each pulse leads to a peak in the axis length which is followed by an exponential decay. The mass spectra show that alkene production peaks immediately after the methanol pulse and quickly dies away. The *c*-axis length after decay is slightly increased with each pulse. This shows that it is necessary to keep feeding methanol into the reactor to maintain good levels of alkene production even though the cages contain some coke.

Analysis of the electron density in the cages by Fourier mapping techniques reveals, as we might predict from the results above, a plot very similar in shape to that of the *c*-axis variation (Fig. 14). Yet again we can see that the *c*-axis variation is linked to the build-up of electron density in the cages. Unfortunately the Raman data from this run are of exceptionally poor quality and could not be meaningfully analyzed to determine the changes in the nature of the coke.

Work by Bleken et al. [45] in which the coke from the MTO process over SAPO-34 was studied using gas chromatography and

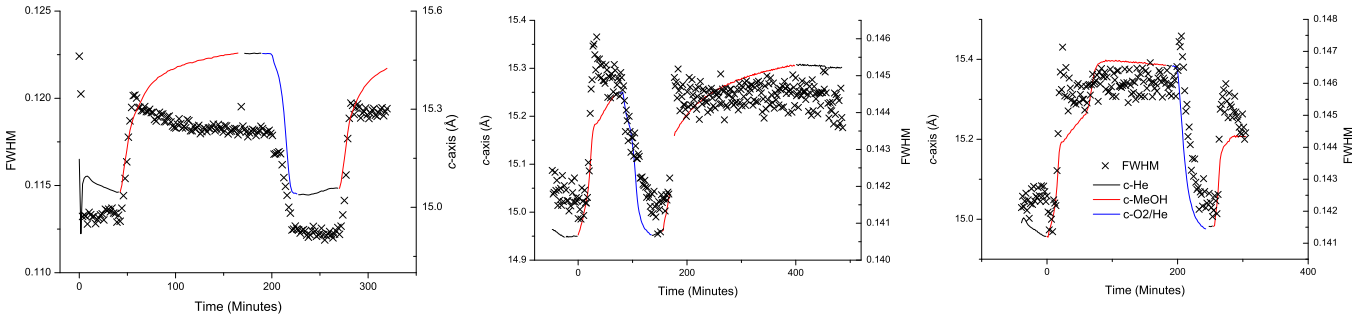

Fig. 12. Plots of FWHM against time for experiments 1–3 (left to right). The *c*-axis curves are shown to indicate the progress of the reaction.

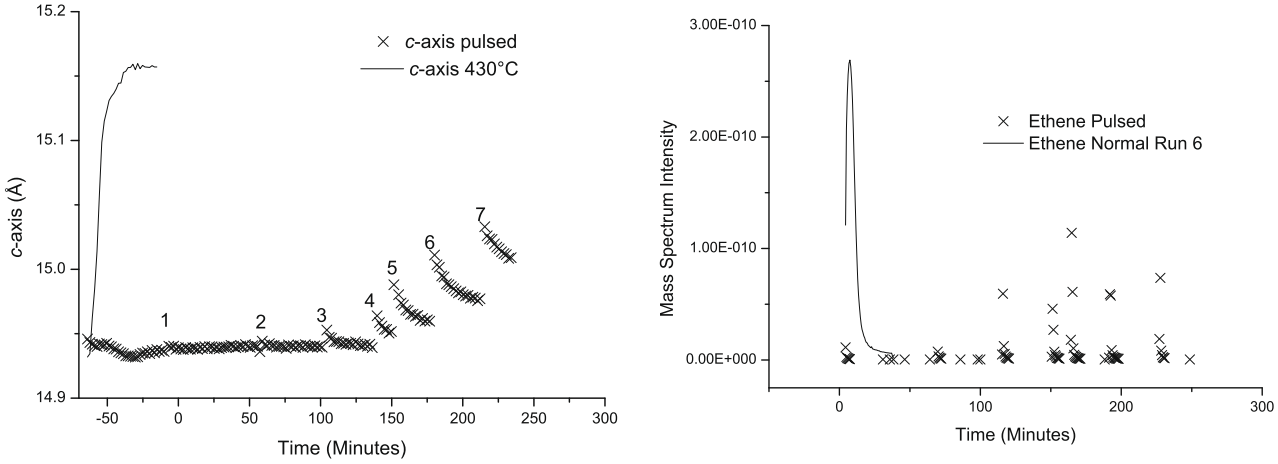

Fig. 13. SAPO-34 *c*-axis variation (left) and propene production in mass spectrum (right) during an experiment in which methanol was added in 7 pulses (addition times marked 1–7, with the first addition at time = 0). The size of the *c*-axis shift (in the *c*-axis plot) and the mass spectrum trace (in the mass spectrum plot) at 430 °C under continuous flow are shown for comparison.

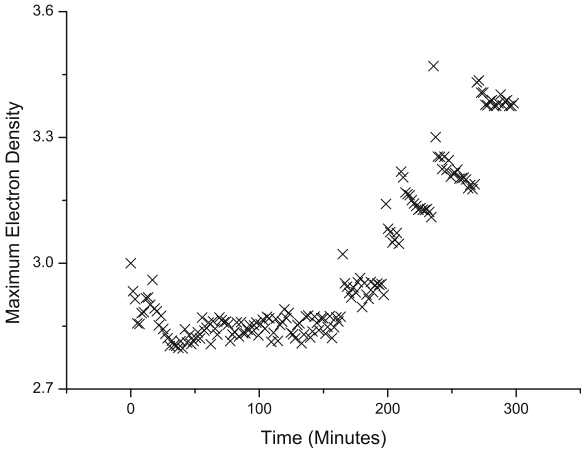

Fig. 14. Variation in the maximum electron density in Fourier maps calculated from the SAPO-34 powder patterns during the pulsed MTO experiment, plotted against time. There is a clear similarity to Fig. 13.

mass spectrometry (GC–MS) took samples of catalyst after 20 min on stream; the feed was then switched to helium and after 60 min a second sample was taken. The samples were dissolved in hydrofluoric acid to destroy the SAPO-34 framework and the organic residues were extracted with dichloromethane and analyzed by GC–MS. The coke found in the second sample contained larger species, such as naphthalenes in place of polymethylated benzenes. This suggests that we might expect to see an increase in *c* after each pulse, which is the opposite of what we observe. It may be that the peaks in *c*-axis length after each pulse are due to large, active and rapidly depleted hexamethylbenzene intermediates. Hexamethylbenzenes are so active that they are rarely seen in GC–MS experiments of the type carried out by Bleken et al. but have been identified as a key intermediate in the MTO process [49]. We also note that the effective time on stream for each of our pulses is short (5–7 min) and that large coke molecules may build up outside the cages.

4. Conclusions

This paper reports the first *in situ* crystallographic investigation of the behaviour of SAPO-34 under real MTO conversion conditions.

The results suggest a strong link between intermediate formation within the cages and expansion of the SAPO-34 unit cell (especially in the *c*-axis direction). Both XRD and Raman show that aromatic coke appears very rapidly and has an immediate effect on the catalyst structure, while the Raman spectra further reveal that graphitic coke begins to develop on the catalyst surface at a relatively early stage. When the MTO process is carried out at lower temperatures (430–450 °C) the structural changes appear to be completely reversible on oxidative regeneration. The development of the FWHM of the (1 0 1) peak indicates that the formation of coke induces strain in the lattice of SAPO-34. The progress of the reaction can be monitored by the *c*-axis length and we have also demonstrated a trend towards the formation of more graphitic coke (probably on the catalyst surface) as the process progresses.

The pulsed experiment is of great interest as it reveals the growth in size of coke species during the reaction. It seems likely that the spikes in the *c*-axis length are caused by the presence of highly active and large methylated intermediate species which are quickly used up leaving inactive species which become larger after each pulse.

These results show the potential of *in situ* synchrotron PXRD as a tool for probing the behaviour of catalysts under real working conditions and also that we can gain complementary information from Raman spectroscopy and mass spectrometry.

Acknowledgments

We thank the Norwegian Research Council and INEOS for funding of the InGAP MTO-RTA project and acknowledge for the use of the SNBL at the ESRF, experiment number 01-02-785 and thank the beam line staff for their assistance. We also thank Professor Unni Olsbye for discussions and providing a copy of Ref. [6] prior to publication and Dr. Andrew Beale for discussions on Raman analysis.

Appendix A. Supplementary material

Supplementary data associated with this article can be found, in the online version, at doi:10.1016/j.jcat.2009.09.027.

References

[1] M. Stöcker, Micropor. Mesopor. Mater. 29 (1999) 3.
[2] B.V. Vora, T.L. Marker, P.T. Barger, H.R. Nilsen, S. Kvisle, T. Fuglerud, in: M. De Pontes, R.L. Espinoza, C.P. Nicolaides, J.H. Scholz, M.S. Scurrell (Eds.), Stud. Surf. Sci. Catal., vol. 107, Elsevier, Amsterdam, 1997, p. 87.
[3] I.M. Dahl, S. Kolboe, Catal. Lett. 20 (1993) 329.
[4] I.M. Dahl, S. Kolboe, J. Catal. 149 (1994) 458.
[5] I.M. Dahl, S. Kolboe, J. Catal. 161 (1996) 304.
[6] B.P.C. Hereijgers, F. Bleken, M.H. Nilsen, S. Svelle, K.P. Lillerud, M. Bjørgen, B.M. Weckhuysen, U. Olsbye, J. Catal. 264 (2009) 77.
[7] G.F. Froment, W.J.H. Dehartog, A. Marchi, Catalysis 9 (1992) 1.
[8] D.M. Bibby, R.F. Howe, G.D. McLellan, Appl. Catal. A 93 (1992) 1.
[9] H. van Bekkum, E.M. Flaningen, P.A. Jacobs, J.C. Jansen, Introduction to Zeolite Science & Practice, Elsevier, Amsterdam, 2001.
[10] D. Mores, E. Stavitski, M. Kox, J. Kornatowski, U. Olsbye, B. Weckhuysen, Chem. Eur. J. 14 (2008) 11320.
[11] P. Norby, U. Schwarz, in: R.E. Dinnebier, S.J.L. Billinge (Eds.), Powder Diffraction Theory and Practice, Royal Society of Chemistry, Cambridge, 2008, p. 439.
[12] R.J. Francis, D. O'Hare, J. Chem. Soc., Dalton Trans. (1998) 3133.
[13] P. Norby, Curr. Opin. Colloid Interf. Sci. 11 (2006) 118.
[14] T. Shido, R. Prins, Curr. Opin. Solid State Mater. Sci. 3 (1998) 330.
[15] M. Milanesio, G. Artioli, A.F. Gualtieri, L. Palin, C. Lamberti, J. Am. Chem. Soc. 125 (2003) 14549.
[16] D. Grandjean, A.M. Beale, A.V. Petukhov, B.M. Weckhuysen, J. Am. Chem. Soc. 127 (2005) 14454.
[17] V. Prevot, V. Briois, J. Cellier, C. Forano, F. Leroux, J. Phys. Chem. Solid 69 (2008) 1091.
[18] E. Boccaleri, F. Carniato, G. Croce, D. Viterbo, W. van Beek, H. Emerich, M. Milanesio, J. Appl. Cryst. 40 (2007) 684.
[19] http://www.esrf.eu/UsersAndScience/Experiments/CRG/BM01/bm01-a.
[20] I.M. Dahl, R. Wendelbo, A. Andersen, D. Akporiaye, H. Mostad, T. Fuglerud, Micropor. Mesopor. Mater. 29 (1999) 59.
[21] A.P. Hammersley, 2004. <http://www.esrf.eu/computing/scientific/FIT2D/>.
[22] A.C. Larson, R.B. Von Dreele, Los Alamos National Laboratory Report, LAUR 86, 1994.
[23] B.H. Toby, J. Appl. Cryst. 34 (2001) 210.
[24] http://www.iza-structure.org/databases/.
[25] A.L. Spek, J. Appl. Cryst. 36 (2003) 7.
[26] G.M. Sheldrick, Acta Crystallogr. A64 (2008) 112.
[27] M. Wojdyr, 2008. <http://www.unipress.waw.pl/fityk/>.
[28] M.G. O'Brien, personal communication.
[29] H. van Koningsveld, J.C. Jansen, Micropor. Mesopor. Mater. 6 (1996) 159.
[30] B.F. Mentzen, Mater. Res. Bull. 27 (1992) 953.
[31] H. van Koningsveld, F. Tuinstra, H. van Bekkum, J.C. Jansen, Acta Crystallogr. B45 (1989) 423.
[32] K. Nishi, A. Hidaka, Y. Yokomori, Acta Crystallogr. B61 (2005) 160.
[33] B.F. Mentzen, P. Gelin, Mater. Res. Bull. 30 (1995) 373.
[34] B.F. Mentzen, F. Lefebvre, Mater. Res. Bull. 32 (1997) 813.
[35] J. Li, G. Xiong, Z. Feng, Z. Liu, Q. Xin, C. Li, Micropor. Mesopor. Mater. 39 (2000) 275.
[36] Y.T. Chua, P.C. Stair, J. Catal. 213 (2003) 39.
[37] M. Bjørgen, U. Olsbye, S. Svelle, S. Kolboe, Catal. Lett. 93 (2004) 37.
[38] Y. Jiang, J. Huang, V. Reddy Marthala, Y.S. Ooi, J. Weitkamp, M. Hunger, Micropor. Mesopor. Mater. 105 (2007) 132.
[39] D. Eisenbach, E. Gallei, J. Catal. 56 (1979) 377.
[40] L. Palumbo, F. Bonino, P. Beato, M. Bjørgen, A. Zecchina, S. Bordiga, J. Phys. Chem. C 112 (2008) 9710.
[41] J. Melsheimer, D. Ziegler, Faraday Trans. 88 (1992) 2101.
[42] M. Bjørgen, F. Bonino, B. Arstad, S. Kolboe, K. Lillerud, A. Zecchina, S. Bordiga, Chem. Phys. Chem. 6 (2005) 232.
[43] M. Bjørgen, F. Bonino, S. Kolboe, K. Lillerud, A. Zecchina, S. Bordiga, J. Am. Chem. Soc. 125 (2003) 15863.
[44] S. Reich, C. Thomsen, Philos. Trans. R. Soc. Lond. 362 (2004) 2271.
[45] F. Bleken, M. Bjørgen, L. Palumbo, S. Bordiga, S. Svelle, K. Lillerud, U. Olsbye, Top. Catal. 52 (2009) 218.
[46] A. Grønvold, K. Moljord, T. Dypvik, A. Holmen, in: H.E. Curry-Dyde, R.F. Howe (Eds.), Stud. Surf. Sci. Catal., vol. 81, Elsevier, Amsterdam, 1994, p. 399.
[47] P. Scardi, in: R.E. Dinnebier, S.J.L. Billinge (Eds.), Powder Diffraction Theory and Practice, Royal Society of Chemistry, Cambridge, 2008, p. 376.
[48] T. Gressmann, A. Leineweber, E.J. Mittemeijer, Philos. Mag. 88 (2008) 45.
[49] B. Arstad, S. Kolboe, J. Am. Chem. Soc. 123 (2001) 8137.